Gaseous Swelling of U_3Si_2 during Steady-State LWR Operation: a Rate Theory Investigation

Yinbin Miao[a,*], Kyle A. Gamble[b], David Andersson[c], Bei Ye[a],
Zhi-Gang Mei[a], Gerard Hofman[a], Abdellatif M. Yacout[a]

[a]*Argonne National Laboratory, Lemont, IL 60439, United States*
[b]*Idaho National Laboratory, Idaho Falls, ID 83415, United States*
[c]*Los Alamos National Laboratory, Los Alamos, NM 87545, United States*

Abstract

Rate theory simulations of fission gas behavior in U_3Si_2 are reported for light water reactor (LWR) steady-state operation scenarios. A model of U_3Si_2 was developed and implemented into the GRASS-SST code based on available research reactor post-irradiation examination (PIE) data, and density functional theory (DFT) calculations of key material properties. Simplified peripheral models were also introduced to capture the fuel-cladding interaction. The simulations identified three regimes of U_3Si_2 swelling behavior between 390 K and 1190 K. Under typical steady-state LWR operating conditions where U_3Si_2 temperature is expected to be below 1000 K, intragranular bubbles are dominant and fission gas is retained in those bubbles. The consequent gaseous swelling is low and associated degradation in the fuel thermal conductivity is also limited. Those predictions of U_3Si_2 performance during steady-state operations in LWRs suggest that this fuel material is an appropriate LWR candidate fuel material. Fission gas behavior models established based on this work are being coupled to the thermo-mechanical simulation of the fuel behavior using the BISON fuel performance multi-dimensional finite element code.

Keywords: silicide fuels, fission gas behavior, rate theory, light water reactor (LWR), steady-state operation

*Tel: +1 (630) 252-7448. Email: ymiao@anl.gov (Y. Miao)

1. Introduction

The nuclear accident in Fukushima following the Great East Japan Earthquake and Tsunami motivated global collaboration in searching for novel nuclear fuel solutions with enhanced accident tolerance [1, 2]. The accident tolerant fuel (ATF) campaign aims to find a novel fuel-cladding combination to replace the current UO_2-zirconium alloy solution. U_3Si_2, a high-temperature stable uranium silicide compound [3], has improved heavy metal density and thermal conductivity compared to UO_2 [4]. These superior properties lead to lower thermal energy storage and lower required enrichment, giving U_3Si_2 the potential to provide excellent accident tolerance while benefiting the fuel cycle with lower enrichment needs or potential fuel life extension. U_3Si_2 is therefore regarded as a promising ATF candidate [5]. Although the fuel performance of U_3Si_2 under research reactor conditions has been investigated extensively [3, 6, 7, 8, 9, 10], little information is available about its behavior in light water reactors (LWRs). In order to qualify U_3Si_2 as an LWR fuel, advanced fuel performance codes must be developed, accounting for various microstructural evolutions..

Fission gas behavior is one of the most important factors influencing fuel performance. Gaseous fission products, primarily Xe, aggregate within the fuels and form intragranular and intergranular bubbles [11]. The bubbles increase the porosity of the fuel materials, resulting in fission gas swelling and a reduction in thermal conductivity [12]. As burnup increases, the accumulation of fission gas atoms eventually leads to the interconnection of intergranular bubbles and the release of fission gas. This further compromises the thermal conductivity and integrity of the fuel pellet, and introduces extra pressure on the cladding.

In order to capture the nucleation, migration, and growth of fission gas bubbles, the Gas Release and Swelling Subroutine for Steady State and Transient (GRASS-SST) code was developed based on rate theory simulations [13]. GRASS-SST has been successfully utilized to replicate the fission gas behavior in multiple types of fuels [14, 15]. Most importantly, this code properly predicted gaseous swelling of UO_2 under LWR conditions [13], and U_3Si_2 under research reactor conditions [16, 17]. This suggests that the GRASS-SST code is suitable for simulating the fission gas behavior of U_3Si_2 under LWR conditions. Therefore, the GRASS-SST code was used for all

fission gas behavior simulations herein.

The following sections describe the rate theory model implementation into the GRASS-SST code, and simulations of U_3Si_2 behavior under LWR steady state conditions. The coupling of GRASS-SST simulations with the thermo-mechanical simulation of the fuel using the BISON code is also discussed.

2. Methodology

2.1. The rate theory model

The fission gas behavior rate theory model in this study was developed for the GRASS-SST code [13]. It is a mechanistic model that focuses on the kinetics of the separate fission gas atoms and bubbles in a polycrystalline nuclear fuel. It is therefore suitable for the fission gas behavior simulation of monolithic nuclear fuels, such as the U_3Si_2 fuel in LWRs considered in this study.

In the GRASS-SST code, the rate theory model describes multiple phenomena contributing to the fission gas behavior, including the generation of gaseous fission products, diffusion of gaseous atoms, nucleation, re-solution, migration, and growth of bubbles, interconnection of intergranular bubbles, interaction between fission gas and defect structures, and fission gas release. The model distinguishes four different categories of fission gas bubbles based on their locations: lattice, dislocation, grain boundary face, and grain boundary edge; the first two account for the intragranular bubbles, whereas the latter two comprise the intergranular bubbles. The kinetics of bubble evolution are simulated by solving a set of coupled nonlinear differential equations:

$$\frac{dC_i^\alpha}{dt} = -a_i^\alpha C_i^\alpha C_i^\alpha - b_i^\alpha C_i^\alpha + e_i^\alpha (i = 1, 2, ..., N; \alpha = 1, 2, 3, 4), \tag{1}$$

where, i is the size class of the bubble, which is related to the number of atoms in a bubble; α represents the location of the bubble: lattice, dislocation, grain-face, and grain-edge, respectively; C_i^α is the number density of α-type bubbles in the ith size class; and the three coefficients a_i^α, b_i^α, and e_i^α are the rate coefficients at which α-type bubbles are lost or added to the ith size class through assorted processes (including bubble coalescence, migration, re-solution, and

nucleation). The rate coefficients depend on multiple material properties and environmental parameters, which are described in detail in Section 2.3.

In the GRASS-SST code, the volumetric strain due to gaseous swelling, ($\frac{\Delta V_{fuel}}{V_{fuel}}$), is calculated as the summation of volumes of gas bubbles of all categories and in all size classes, namely,

$$\frac{\Delta V_{fuel}}{V_{fuel}} = \sum_{i=1}^{N} \sum_{\alpha=1}^{4} C_i^{\alpha} v_i^{\alpha}, \tag{2}$$

where, v_i^{α} is the volume of an α-type bubble in the ith size class. In the rate theory model, the size class is designated based on the number of atoms contained in the bubbles. Thus, the volume of a bubble can be determined by the equation of state (EOS) of the fission gas. Here, the modified hard sphere EOS derived by Ronchi et al. is adopted for bubble size computation [18]:

$$\frac{4}{3RT}\pi r^3(p + 2\gamma/r) = Z^{hs}(y) - dv_0 f(T) + \Delta Z, \tag{3}$$

where, p is the hydrostatic stress or pressure; γ is the surface energy of the fuel material; r is the bubble radius; R is the gas constant; and T is the thermodynamic temperature. The right hand side (RHS) of Equation 3 accounts for the amount of gas atoms (in moles) in the bubbles and the effects of the hard sphere atomic potential [18].

2.2. Steady-state model parameterization

Fuels in LWRs experience higher operating temperatures than those in research reactors. Thus, thermally-activated diffusion of Xe plays a more important role in the fission gas behavior under LWR conditions, whereas radiation-enhanced diffusion (RED) typically dominates Xe diffusion under research reactor conditions. The diffusivity of a single Xe atom in U_3Si_2 has been assessed by means of density functional theory (DFT) using the Vienna Ab-initio Simulation Package (VASP) [19, 20] with projector augment-wave (PAW) method and Perdew-Burke-Ernzerhof (PBE) potentials for the exchange-correlation potentials and a Hubbard U parameter for the uranium $5f$ electrons [21], following the methodology used in Refs. [22, 23]. In tetragonal structure crystals such as U_3Si_2, migration of a Xe atom through the a-b plane and c-axis differs due to the asymmetric atomic structure. The migration enthalpies of a series of possible migration

routes [24] were calculated using DFT and the nudged elastic band method in VASP [25]. Due to computational complexity, it is challenging to calculate the precise contributions of entropy to diffusion. Instead, the Frenkel entropy was approximated to be $5k_B$ and the vacancy binding entropy -$1k_B$, where k_B is the Boltzmann constant. The attempt frequency for migration jumps was assumed to be 1×10^{13} Hz. The diffusivity of Xe through a specific migration route can be calculated and compared with those through other routes from $D = \nu a^2 Z exp(-G_a/k_B T)/6$, where ν is the attempt frequency; a is the jump distance; Z is the number of site that the Xe atom can jump to; and G_a is the activation free energy given by the migration enthalpy and the defect formation and binding energies. It was found that the migration of a Xe atom from one U vacancy to another U vacancy along the c-axis overwhelmingly dominates the diffusion of Xe in U_3Si_2, whereas the diffusion of Xe in the a-b plane is suppressed. Xe diffusion in U_3Si_2 is therefore modeled as a one-dimensional diffusion, by $\overline{\overline{D}} = diag\{0, 0, D_3\}$. To take this anisotropy in diffusion into account, an effective three-dimensional diffusivity, $D_{eff} = D_3/3$, was used in the GRASS-SST rate theory model, where spherical grain shape and isotropic Xe diffusion are assumed. In fact, adoption of the effective three-dimensional diffusivity yields the same steady-state Xe concentration in this rate theory model with a uniform Xe source term.

According to Equation 3, the size of fission gas bubbles has a considerable dependence on the surface energy of the fuel material. Hence, a credible estimate of the surface energy of U_3Si_2 is crucial for the accurate prediction of the gaseous swelling strain. Unfortunately, due to a lack of related data, little information about the surface energy of U_3Si_2 can be gleaned from existing experimental data. Thus, DFT calculations were utilized to determine the surface energies of a series of surfaces with various Miller's indices. The DFT calculations were performed using the same parameters described in the previous paragraph. The surface energy was found to vary from 1.16 J/m^2 to 1.48 J/m^2, depending on the crystallographic orientation of the surface. For instance, the {100} surface has a surface energy of 1.48 J/m^2, while the {001} surface has a surface energy of 1.43 J/m^2. For the sake of simplicity, an average surface energy of 1.32 J/m^2 was used in this study for all fission gas behavior simulations under LWR conditions.

Although abundant in-pile irradiation data are available for U_3Si_2, the majority of those

results were obtained under research reactor conditions [6, 10]. That is, the existing data usually involve a lower irradiation temperature ($< 300°C$) and higher fission density (due to higher enrichment) compared to LWR conditions. Under research reactor conditions, the gas bubbles are invisible in scanning electron microscopy (SEM) images until the fission density exceeds a threshold value. Once the threshold fission density is achieved, breakaway swelling occurs due to the formation of large fission gas bubbles visible in SEM, which is known as the "knee" phenomenon [10]. Under LWR conditions, however, the maximum burnup of U_3Si_2 is expected to be around 5%, which is far lower than the threshold of the "knee" phenomenon. Therefore, only the experimental data measured before reaching the threshold were taken into consideration for rate theory parameterization. The research reactor data were used to fit key rate theory parameters that cannot be properly assessed by DFT calculations. In the research reactor data below the threshold, intragranular bubbles dominate the gaseous swelling, while the contribution of intergranular bubbles is negligible. Additionally, as the research reactor data involve the dispersion fuel form, wherein the U_3Si_2 particles are embedded in an Al matrix, an 8.5 MPa hydrostatic stress was assumed, which is the effective yield stress of Al at research reactor temperatures considering radiation creep [26].

Based on the computational and experimental approaches described above, values of the key parameters in the GRASS-SST rate theory model during steady-state operation were determined as listed in Table 1. D_0 and Q are the pre-exponential coefficient and activation energy of thermally-activated Xe atom diffusivity in U_3Si_2, respectively; D_g^{RED} is the coefficient of RED of single Xe atoms; f_n is the bubble nucleation factor; b_0 is the bubble re-solution rate coefficient in the lattice; γ is the surface energy of the fuel material; gbr(1) is the multiplication factor to obtain effective radiation-induced re-solution of gas atoms from a grain face; and χ is the enhancement factor of gas atom's RED on grain boundaries. The computational and experimental references used for parameter optimization concentrate on fission gas behavior within the lattice. Thus, only those material parameters that are involved in intragranular bubble evolution, such as b_0 and D_g^{RED}, are expected to be accurately optimized, whereas the grain boundary related parameters, including gbr(1) and χ, are merely within reasonable empirical ranges for U-Mo and UO_2 fuels.

The limitations of this parameter set will be discussed late in the paper.

Table 1: Values of key parameters in the rate theory model used by the GRASS-SST code

Paramerer	D_0	Q	D_g^{RED}	f_n	b_0	γ	$gbr(1)$	χ
Unit	m^2/s	eV	m^5	n/a	m^3	J/m^2	n/a	n/a
Value	7.73×10^{-7}	1.68	1.0×10^{16}	0.01	1.0×10^{-25}	1.32	1.00	2000

2.3. Steady-State LWR Conditions

As mentioned before, LWRs operate at higher temperatures and achieve lower fuel burnup than research reactors. In order to examine the fuel performance of U_3Si_2 in LWRs, the conditions modeled by the GRASS-SST code must be adjusted accordingly. For consistency and simplicity, the majority of the LWR condition parameters were adopted from Metzger et al.'s BISON simulation work [27]. The key LWR conditions are listed in Table 2.

Table 2: LWR conditions adopted in this study

Parameter	Unit	Value
Linear average power [27]	W/cm	200
Fast neutron flux [27]	n/m^2·s	9.50×10^{17}
Coolant pressure [27]	MPa	15.5
Coolant temperature [27]	K	530
Fill gas initial pressure [27]	MPa	2.0
Initial fuel density [27]	%	95
Power	MW/tU	35.28
Maximum burnup	MWD/tU	45,000

Cylindrical fuel pellets without a central void were clad in Zircaloy-4. The Zircaloy cladding was selected rather than an advanced cladding solution such SiC/SiC or FeCrAl, proposed for used with ATF, to provide direct comparison with the conventional UO_2-zirconium alloy solution. The pellet diameter was 8.2 mm. An 80 micron gap between the fuel pellets and cladding was filled with 2.0 MPa helium gas. Detailed temperature profiles and other operational data were taken from Ref. [27]. The steady-state analysis was performed with a constant power for 3.5 years to a final burnup of 45,000 MWD/tU.

2.4. Models of Peripheral Parameters

In the steady-state simulation, other simplified models were also adopted (in addition to the GRASS-SST rate theory model) to assess the peripheral effects, especially the cladding effects, under LWR conditions. Details of these peripheral models follow.

The hydrostatic pressure of the fuel is influenced by the helium fill gas until gap closure. As the fill gas does not experience extreme conditions, such as ultrahigh pressure or temperature, the behavior of helium was governed by the ideal gas EOS in this study. The helium gas was assumed to maintain a 650 K constant temperature, while the gas volume was determined by considering the plenum and the deformation of both the cladding and fuel. The densification of the fuel was assessed by the empirical ESCORE model [27]. The thermal expansion coefficient of the U_3Si_2 fuel was selected to be 1.5×10^{-5} K^{-1} [3]. The solid fission product swelling was assumed to be proportional to the fission density with a swelling rate of 0.38% per 10^{27} fission/m^3 [6].

The Zircaloy-4 cladding temperature was assumed to maintain a 590 K constant temperature. The cladding was considered to undergo perfect plastic deformation once the yielding stress (145 MPa) was exceeded. The Young's modulus at this temperature is 86.2 GPa. In addition, the radiation creep rate, $\dot{\varepsilon}$ (in percent per hour), was governed by Watkin's empirical equation for Zircaloy [28]:

$$\dot{\varepsilon} = 3.98 \times 10^{-15} \phi^{0.85} sinh(1.67 \times 10^{-2} \sigma) exp(-14000/RT), \tag{4}$$

where, ϕ is fast neutron (>1 MeV) flux (n/m^2·s), σ is stress (MPa), R is the gas constant (1.987 cal/k·mol), and T is the thermodynamic temperature (K).

The temperature difference between the fuel centerline and its surface was taken to be 190 K as predicted by the BISON simulation, with the fuel temperature having a parabolic profile. The fuel surface temperature was assumed to be a linear function of the gap width [27].

The GRASS-SST code was revised to enable a restart function to allow for the tight coupling between the fission gas behavior simulation and the aforementioned peripheral models. A variable timestep was adopted to ensure the convergence of the coupling.

3. Results and Discussions

3.1. Steady-State Gaseous Swelling without Cladding Restraint

The temperature and temperature gradient effects on the fission gas behavior were investigated before introducing any peripheral models. For simplicity, a single-element fuel pellet setup was used first. Additionally, the helium fill gas was assumed to maintain its 2 MPa pressure regardless of the temperature variation of the fuel pellet. Fission gas behavior was examined as a function of fuel temperature in increments of 10 K, and four representative temperature gradients (0 K/mm, 20 K/mm, 40 K/mm, and 60 K/mm) were examined. The fission gas swelling and release scenarios assessed by the GRASS-SST rate theory model at 45,000 MWd/tU are shown in Figure 1. The gaseous swelling originating from both intragranular (lattice) and intergranular (grain boundary face and edge) bubbles were computed and illustrated separately. At temperatures between 390 K (research reactor temperature) and 1190 K (accident scenario), three regimes of fission gas behavior can be distinguished. When the average fuel temperature is below approximately 750 K (Regime I), the gaseous swelling is comparable to that observed in research reactors prior to the occurrence of the "knee" point (point of accelerated swelling). When the temperature exceeds approximately 750 K but is still lower than a threshold around 1000 K (Regime II), the gaseous swelling slowly increases with the fuel temperature. However, in this regime, the swelling is still controllable as intragranular bubbles remain dominant. As the fuel temperature increases beyond this threshold, the grain boundary bubbles start to contribute considerably to the gaseous swelling. Consequently, it is in this regime that the gaseous swelling first becomes severe. As the temperature continues to increase, the interconnections of intergranular bubbles eventually form channels for gas release. Once those channels are formed, the gaseous swelling drops dramatically. The temperature of the threshold between Regimes II and III is dependent on the temperature gradient, as shown in Figure 2. In the absence of a temperature gradient, Regime III does not appear until 1490 K. However, for a temperature gradient greater than 0.5 K/mm, the threshold drops with increasing temperature gradient, and is in the range of approximately 1000 K to 1150 K. As mentioned previously, the parameterization of the intergranular bubbles is not optimized due to the lack of experimental data. Hence, the quantitative

information in Regime III should not be considered reliable. Nevertheless, the qualitative features of the three divided regimes are credible.

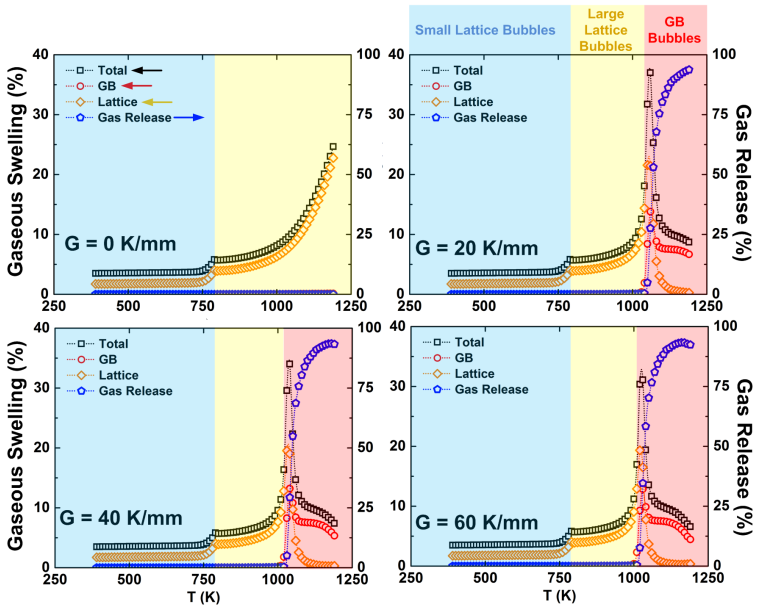

Figure 1: Fission gas behavior at different temperatures and temperature gradients

More information about the competition between intragranular and intergranular bubbles at various temperatures and temperature gradients is gleaned by analyzing their size distribution and number density, summarized in Figure 3. In Regime I, the intragranular bubbles have a monomodal size distribution peaking at approximately 1.5 nm in radius. In Regime II, enhanced Xe diffusion causes the formation of larger intragranular bubbles. The large intragranular bubbles (around 20 nm in radius) form, leading to a bimodal size distribution and significantly increasing the mean radius of intragranular bubbles. The appearance of these large intragranular bubbles accounts for the prominent but controllable increase in gaseous swelling in Regime II. In Regime III, fission gas starts to reach grain boundaries to form intergranular bubbles, whereas the growth of intragranular bubbles is inhibited.

Because of the existence of these three temperature regimes, the fission gas behavior in U_3Si_2 under LWR conditions can be sensitive to fuel temperature and temperature gradient.

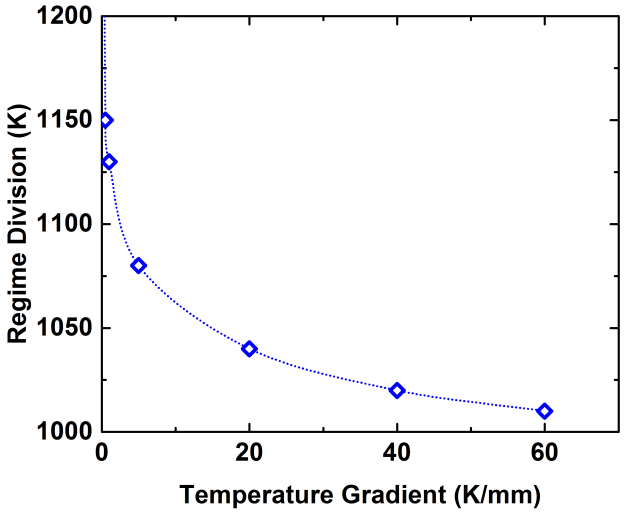

Figure 2: The division between Regimes II and III (temperature at boundary between the two regimes) versus temperature gradient within the fuel pellet (the dashed line is given only for eye-guiding purpose)

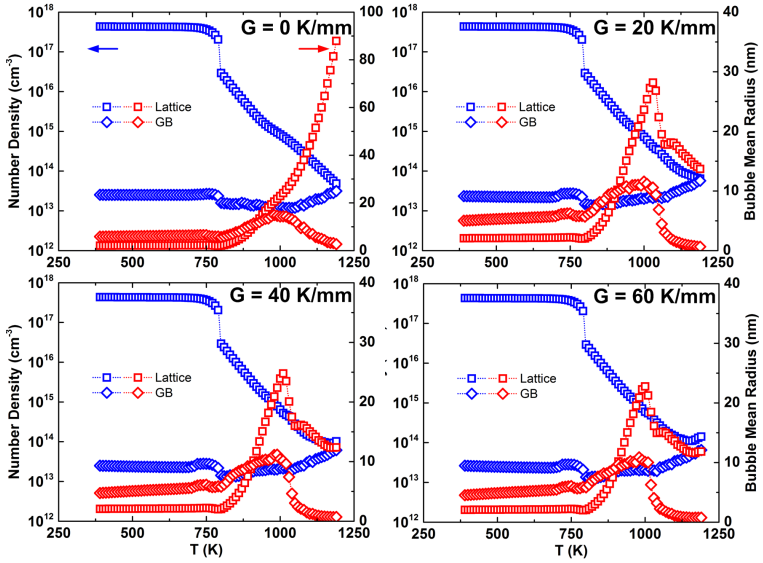

Figure 3: Mean size and number density comparison of fission gas bubbles at different temperatures and temperature gradients

Considering the significant temperature difference within the pellet, the centerline region and the surface region are likely to be in different temperature regimes. Meanwhile, assuming a parabolic temperature distribution in the radial direction, the temperature gradient near the surface is much larger than that in the center. While single-element simulation is suitable for analyzing the contributions of temperature, temperature gradient, and burnup to fission gas behavior, mesh refinement of the computational elements was needed to improve the fission gas swelling predictions, especially at the near surface region. The temperature gradient effect becomes important only when the temperature is in excess of 1000 K. Using a refined mesh, the temperature dependence of the fission gas behavior was re-examined. The results are shown in Figures 4 and 5. Notice that with multiple mesh elements, each element has its own temperature and temperature gradient. Consequently, elements at various radial positions can be within different temperature regimes.

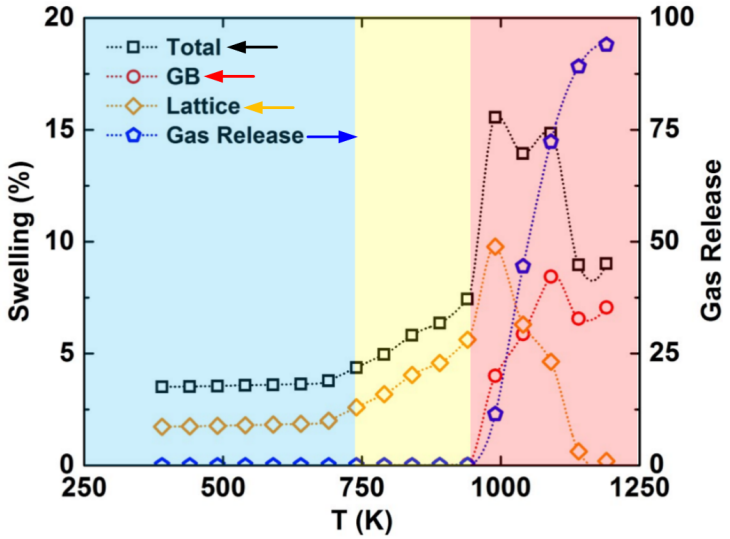

Figure 4: Three temperature regimes of fission gas behavior in U_3Si_2 using a 10-element simulation

3.2. Development of BISON Correlations

As was observed in this study, gaseous swelling in U_3Si_2 under LWR conditions is a complex process that is affected by a series of parameters including temperature, temperature gradient,

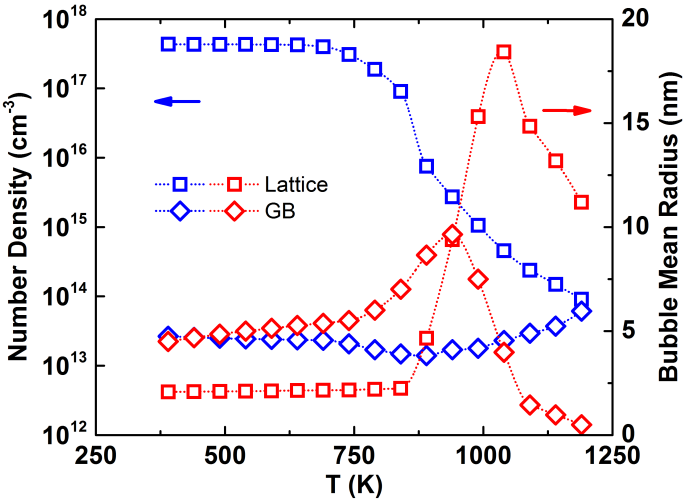

Figure 5: Mean size and number density of fission gas bubbles in U_3Si_2 using a 10-element simulation

hydrostatic pressure, and fission density. However, the existing gaseous swelling correlation (used in BISON) was developed based on limited research reactor data and is only dependent on fission density [27]. In order to improve the gaseous swelling model used by finite element method (FEM) codes such as BISON, a rate theory based gaseous swelling correlation was established using the swelling strains predicted by the GRASS-SST code. Thus, it was assumed that the gaseous swelling in U_3Si_2 is only dependent on three variables: temperature (T), temperature gradient (G), and fission density (f). The temperature or temperature gradient in an element was assumed not to vary significantly. To conservatively estimate gaseous swelling, the highest temperature and temperature gradient during the entire pellet element segment history were used for the values of T and G, respectively.

A typical LWR fission rate (see Table 2) was used to generate the swelling data for fitting, so the application of this correlation should not be far from the typical LWR conditions. Thus, 81 temperature points (390 K to 1190 K in 10 K intervals), 11 temperature gradient points (0, 1, 5, 10, 20, 30, 40, 50, 60, 70, and 80 K/mm), and up to 1.29×10^{21} fission/cm^3 fission density (256 data points, up to 5% burnup), were used to calculate the gaseous swelling using the

GRASS-SST code. As no simple functions are capable of capturing all the details of gaseous swelling's dependence on T, G, and f, tricubic interpolation was used to establish the correlation [29]. The interpolated correlation has C^1 continuity in the T-G-f space, and replicated the GRASS-SST results with constant temperatures and temperature gradients. This correlation has been embedded in the BISON code. Detailed parameterization and documentation will be available in the BISON database soon.

In addition to the gaseous swelling strain, the GRASS-SST code calculates detailed size distribution and number density of intragranular and intergranular bubbles. These can in turn be used to deduce the reduction in thermal conductivity due to fission gas bubbles. Multiple models have been reported to describe the influence of intragranular bubbles on thermal conductivity [30, 31, 32, 33, 12]. A model based on U_3Si experimental data was used in this study [34]:

$$\kappa_{intra} = \frac{1-p}{1+0.9p}, \tag{5}$$

where κ_{intra} is the thermal conductivity degradation factor due to intragranular bubbles and p is the volume fraction of intragranular bubbles. Although some thermal conductivity degradation models due to intergranular bubbles were recently reported [33, 12], they require as input the Kapitza thermal resistance of the grain boundary, which is a material property unknown for U_3Si_2. Thus, the development of the thermal conductivity degradation factor due to intergranular bubbles, κ_{inter}, is difficult to quantify. Fortunately, during steady-state LWR operation, as predicted in this study, fission gaseous swelling is overwhelmingly dominated by intragranular bubbles. Therefore, the κ_{intra} correlation was developed based on the rate theory results and tricubic interpolation. Implementation of this correlation into the BISON code is in process.

3.3. Steady-State Gas Swelling Affected by Cladding

The cladding effects on the fission gas behavior during steady-state operation were considered using the peripheral models introduced previously. The swelling strain was then compared to that obtained using the original correlation in the BISON code based on the low temperature research reactor data (see Figure 6). The rate theory model yields a gaseous swelling prediction

that is higher than the original BISON correlation at low and intermediate burnup. This is due to the fact that, under LWR conditions, the temperature range almost fits within Regime II in Figure 5. Hence, mechanism in the low temperature conditions (Regime I) in research reactors, the intragranular bubbles in LWRs can be as large as tens of nm. The size distribution of the gas bubbles predicted by the GRASS-SST simulation with cladding (see Figure 7) indicates an apparently bimodal distribution. When the evolution of average bubble size and number density is analyzed separately for two size groups of intragranular bubbles, as indicated in Figure 8, the bubble growth mechanisms are unveiled. It is clear that small intragranular bubbles (r <2 nm) have a saturated size at a radius of approximately 1.5 nm, and their number density increases with burnup. On the other hand, large intragranular bubbles (r >2 nm,) have a saturated number density at approximately 2×10^{21} m^{-3}, while their size continues to increase with burnup. In the high burnup regime, the original BISON correlation, which was fitted to research reactor data, is influenced by the "knee" phenomenon. Therefore, the original BISON correlation overestimates the gaseous swelling compared to the rate theory results.

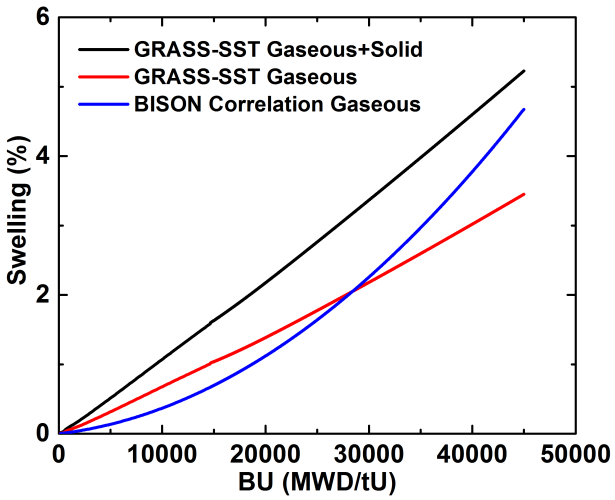

Figure 6: Comparison between the rate theory simulation and the original BISON correlation.

Due to the swelling of the fuel pellet and creep-down of the cladding, gap closure occurs

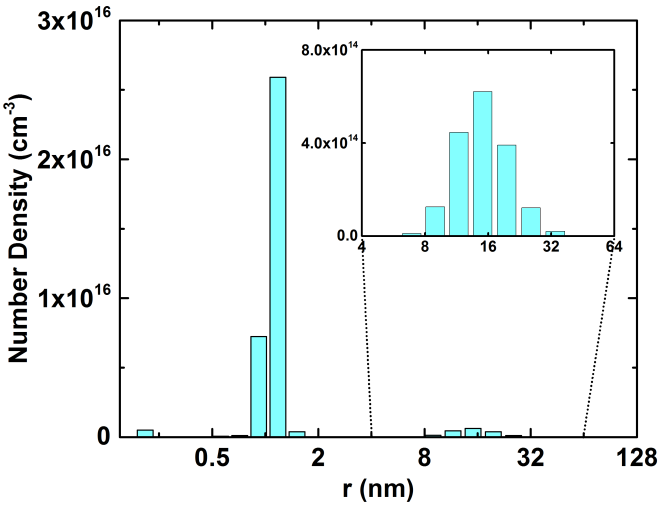

Figure 7: Bimodal size distribution of intragranular fission gas bubbles under LWR conditions with cladding effect.

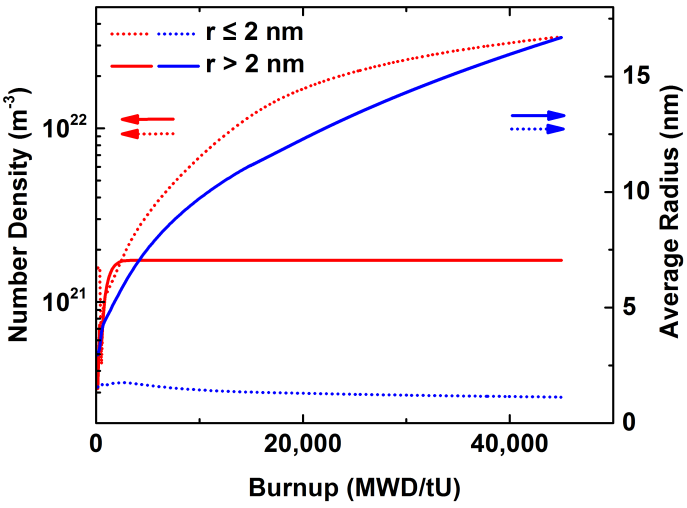

Figure 8: Evolution of average size and number density of the intragranular bubbles with bimodal size distribution.

at approximately 14,000 MWd/tU. Soon after the gap closure, the hoop stress of the Zircaloy-4 cladding inverts (see Figure 9), leading to the consequent reversal of the creep direction. As the hoop stress increases, the hydrostatic pressure of the fuel also increases. However, this high pressure seems to not effectively relieve the gaseous swelling shown in Figure 6. This is because those intragranular bubbles with radii around or below tens of nm are still too small to compress. Instead, the bubble size is controlled by the surface energy of the fuel.

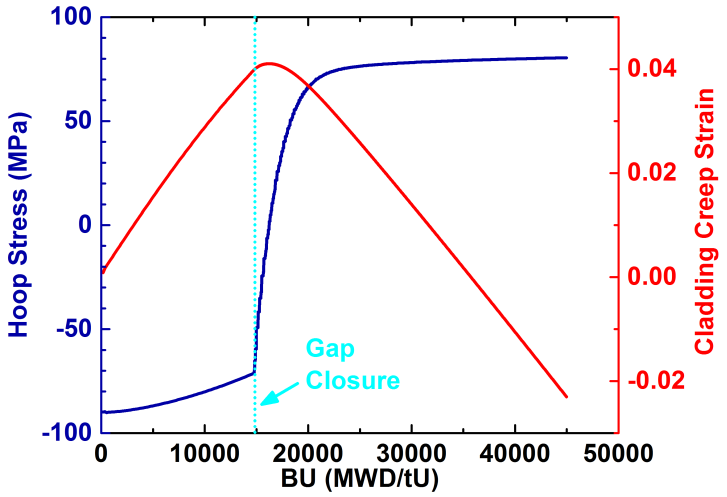

Figure 9: The hoop stress and corresponding creep strain of the Zircaloy-4 cladding.

3.4. Sensitivitiy Analysis of the Steady-State Rate Theory Model

In order to examine the reliability of the rate theory model developed in this study, the sensitivity of the key parameters (listed in Table 3) was analyzed by altering those parameters and then comparing the gaseous swelling strain at the ultimate burnup. The LWR conditions with cladding as described previously were used as conditions of the reference state. The results of this sensitivity analysis are listed in Table 3. As fission gas bubble evolution is almost entirely within the grains rather than on the grain boundaries, the gaseous swelling behavior at LWR conditions is sensitive to the parameters that are related to intragranular bubbles, such as Xe diffusivity

Table 3: Sensitivity analysis on key parameters at LWR conditions (reference: $\Delta V/V$=5.2265%)

Parameter	Unit	Value	$\Delta V/V$ (%)	Difference (%)
D_0	cm^2/s	7.73×10^{-2}	5.4519	4.31
		7.73×10^{-4}	5.1421	-1.61
Q	eV	3.36	5.1460	-17.54
		0.84	7.4361	42.28
D_g^{RED}	cm^5	1.0×10^{-25}	5.2723	8.76
		1.0×10^{-27}	5.1569	-1.33
f_n	n/a	0.1	4.9514	-5.26
		0.001	5.4851	4.95
b_0	cm^3	1.0×10^{-18}	6.1096	16.90
		1.0×10^{-20}	4.7743	-8.65
γ	J/m^2	5	4.0436	-22.63
		0.2	8.9119	70.51
gbr(1)	n/a	10	5.2387	0.23
		0.1	5.2462	0.38
χ	n/a	20,000	5.2272	0.01
		200	5.2280	0.03

within grains, nucleation/re-solution coefficients, and surface energy. Meanwhile, the influence of those grain boundary related parameters, gbr(1) and χ in particular, is marginal. At LWR temperatures, thermally-activated diffusion exceeds the RED of Xe, becoming the dominant driving force of bubble evolution. As a result, the swelling strain is more sensitive to D_0 and Q than D_g^{RED}. It is worth mentioning that constraint by the Zircaloy-4 cladding limits the swelling behavior in some cases that involve prominent increases in swelling rate. For example, a decrease in surface energy is expected to lead to a large increase in swelling strain. However, hydrostatic stress from the cladding relieves the severe inflation due to the absence of surface constraint.

4. Conclusions

In this study, the GRASS-SST rate theory model was optimized for U_3Si_2 fuel material under LWR conditions based on both research reactor experimental data and DFT calculations. The model was then used to predict the fission gas behavior of U_3Si_2 under LWR conditions with focus on steady-state behavior of U_3Si_2. Intragranular bubbles with bimodal size distribution were found to dominate the gaseous swelling of U_3Si_2 in LWRs, whereas the contribution from

intergranular bubbles and gas release was marginal. A steady-state gaseous swelling correlation was developed for use in the BISON code, replacing the original correlation based only on research reactor data. Simplified peripheral models were also established to couple with the rate theory code to investigate the influence of the cladding. This also facilitates future coupling of the GRASS-SST code and FEM codes (e.g. BISON). According to the rate theory simulation, under steady-state LWR operating conditions, fission gas is retained in intragranular bubbles. Thus, gaseous swelling in U_3Si_2 is benign and controllable during steady-state operation. To further qualify U_3Si_2 as an ATF, its fission gas behavior during power transients, especially loss-of-coolant accidents (LOCAs) must be investigated in the future.

5. Acknowledgments

This work was funded by the Accident Tolerant Fuel High-Impact Problems (ATF-HIP) of the U.S. Department of Energy (DOE)'s Nuclear Energy Advanced Modeling and Simulation (NEAMS) program. The efforts involving Argonne National Laboratory were sponsored under Contract No. DE-AC02-06CH11357 between UChicago Argonne, LLC and the U.S. Department of Energy. The submitted manuscript has been authored by a contractor of the U.S. Government under Contract DE-AC07-05ID14517. Accordingly, the U.S. Government retains a non-exclusive, royalty free license to publish or reproduce the published form of this contribution, or allow others to do so, for U.S. Government purposes. Los Alamos National Laboratory, an affirmative action/equal opportunity employer, is operated by Los Alamos National Security, LLC, for the National Nuclear Security Administration of the U.S. Department of Energy under Contract No. DE-AC52-06NA25396.

References

[1] S. J. Zinkle, K. A. Terrani, J. C. Gehin, L. J. Ott, L. L. Snead, Journal of Nuclear Materials 448 (2014) 374–379.

[2] J. Carmack, F. Goldner, S. M. Bragg-Sitton, L. L. Snead, in: Proc. 2013 LWR Fuel Performance Meeting/TopFuel 2013, pp. 15–19.

[3] H. Shimizu, The properties and irradiation behavior of U3Si2, Atomics International, 1965.

[4] J. White, A. Nelson, J. Dunwoody, D. Byler, D. Safarik, K. McClellan, Journal of Nuclear Materials 464 (2015) 275–280.

[5] J. Carmack, K. Barrett, H. MacLean-Chichester, Light Water Reactor Accident Tolerant Fuels Irradiation Testing, Technical Report, Idaho National Laboratory (INL), Idaho Falls, ID (United States), 2015.

[6] G. L. Hofman, Journal of Nuclear Materials 140 (1986) 256–263.

[7] M. Finlay, G. Hofman, J. Snelgrove, Journal of nuclear materials 325 (2004) 118–128.

[8] A. Leenaers, S. Van den Berghe, E. Koonen, P. Jacquet, C. Jarousse, B. Guigon, A. Ballagny, L. Sannen, Journal of nuclear materials 327 (2004) 121–129.

[9] A. Leenaers, E. Koonen, Y. Parthoens, P. Lemoine, S. Van den Berghe, Journal of Nuclear Materials 375 (2008) 243–251.

[10] Y. S. Kim, G. Hofman, J. Rest, A. Robinson, Journal of Nuclear Materials 389 (2009) 443–449.

[11] G. L. Hofman, Y. S. Kim, Nuclear Engineering and Technology 37 (2005) 299–308.

[12] M. R. Tonks, X.-Y. Liu, D. Andersson, D. Perez, A. Chernatynskiy, G. Pastore, C. R. Stanek, R. Williamson, Journal of Nuclear Materials 469 (2016) 89–98.

[13] J. Rest, GRASS-SST: a comprehensive, mechanistic model for the prediction of fission-gas behavior in UO/sub 2/-base fuels during steady-state and transient conditions, Technical Report, ANL-78-53, Argonne National Laboratory, Illinois, USA, 1978.

[14] D. Yun, J. Rest, G. L. Hofman, A. M. Yacout, Journal of Nuclear Materials 435 (2013) 153–163.

[15] B. Ye, J. Rest, Y. S. Kim, G. Hofman, B. Dionne, Nuclear Technology 191 (2015) 27–40.

[16] J. Rest, G. Hofman, in: Fundamental Aspects of Inert Gases in Solids, Springer, 1991, pp. 443–456.

[17] J. Rest, Journal of nuclear materials 325 (2004) 107–117.

[18] C. Ronchi, Journal of Nuclear Materials 96 (1981) 314–328.

[19] G. Kresse, J. Furthmüller, Physical review B 54 (1996) 11169.

[20] G. Kresse, D. Joubert, Physical Review B 59 (1999) 1758.

[21] S. Dudarev, D. N. Manh, A. Sutton, Philosophical Magazine B 75 (1997) 613–628.

[22] M. J. Noordhoek, T. M. Besmann, D. Andersson, S. C. Middleburgh, A. Chernatynskiy, Journal of Nuclear Materials 479 (2016) 216–223.

[23] S. Middleburgh, R. Grimes, E. Lahoda, C. Stanek, D. Andersson, Journal of Nuclear Materials 482 (2016) 300–305.

[24] A. D. Andersson, Density functional theory calculations of defect and fission gas properties in U-Si fuels, Technical Report, Los Alamos National Laboratory (LANL), 2016.

[25] G. Mills, H. Jónsson, G. K. Schenter, Surface Science 324 (1995) 305–337.

[26] J. Rest, The DART dispersion analysis research tool: A mechanistic model for predicting fission-product-induced swelling of aluminum dispersion fuels. Users guide for mainframe, workstation, and personal computer applications, Technical Report, ANL-95/36, Argonne National Laboratory, Illinois, USA, 1995.

[27] K. Metzger, T. Knight, R. Williamson, in: Proceedings of the International Congress on Advances in Nuclear Power

Plants–ICAPP 2014, Charlotte, NC.

[28] B. Watkins, D. Wood, in: Applications-Related Phenomena in Zirconium and its Alloys, ASTM International, 1969.

[29] F. Lekien, J. Marsden, International Journal for Numerical Methods in Engineering 63 (2005) 455–471.

[30] R. Progelhof, J. Throne, R. Ruetsch, Polymer Engineering & Science 16 (1976) 615–625.

[31] P. Nikolopoulos, G. Ondracek, Journal of Nuclear Materials 114 (1983) 231–233.

[32] J. K. Carson, S. J. Lovatt, D. J. Tanner, A. C. Cleland, International Journal of Heat and Mass Transfer 48 (2005) 2150–2158.

[33] M. R. Tonks, P. C. Millett, P. Nerikar, S. Du, D. Andersson, C. R. Stanek, D. Gaston, D. Andrs, R. Williamson, Journal of Nuclear Materials 440 (2013) 193–200.

[34] J. Hastings, J. MacEwan, L. Bourque, Journal of the American Ceramic Society 55 (1972) 240–242.